

Approaching optimal entangling collective measurements on quantum computing platforms

Lorcán O. Conlon,^{1,*} Tobias Vogl,^{2,3} Christian D. Marciniak,⁴ Ivan Pogorelov,⁴ Simon K. Yung,¹ Falk Eilenberger,^{2,5,6} Dominic W. Berry,⁷ Fabiana S. Santana,⁸ Rainer Blatt,^{4,9} Thomas Monz,^{4,10} Ping Koy Lam,^{1,11,12,†} and Syed M. Assad^{1,11,‡}

¹*Centre for Quantum Computation and Communication Technology, Department of Quantum Science, Australian National University, Canberra, ACT 2601, Australia.*

²*Institute of Applied Physics, Abbe Center of Photonics, Friedrich-Schiller-Universität Jena, 07745 Jena, Germany*

³*Cavendish Laboratory, University of Cambridge, JJ Thomson Avenue, Cambridge CB3 0HE, United Kingdom*

⁴*Institut für Experimentalphysik, 6020 Innsbruck, Austria*

⁵*Fraunhofer-Institute for Applied Optics and Precision Engineering IOF, 07745 Jena, Germany*

⁶*Max Planck School of Photonics, 07745 Jena, Germany*

⁷*School of Mathematical and Physical Sciences, Macquarie University, Sydney, NSW 2109, Australia*

⁸*Amazon Web Services, Canberra, ACT 2601, Australia*

⁹*Institute for Quantum Optics and Quantum Information, 6020 Innsbruck, Austria*

¹⁰*Alpine Quantum Technologies (AQT), 6020 Innsbruck, Austria*

¹¹*School of Physical and Mathematical Sciences, Nanyang Technological University, Singapore 639673, Republic of Singapore*

¹²*Institute of Materials Research and Engineering, Agency for Science Technology and Research (A*STAR), 2 Fusionopolis Way, 08-03 Innovis 138634, Singapore*

Entanglement is a fundamental feature of quantum mechanics and holds great promise for enhancing metrology and communications. Much of the focus of quantum metrology to date has been on generating highly entangled quantum states which offer better sensitivity, per resource, than what can be achieved classically. However, to reach the ultimate limits in multi-parameter quantum metrology and quantum information processing tasks, collective measurements, which generate entanglement between multiple copies of the quantum state, are necessary. Here we experimentally demonstrate theoretically optimal single-copy and two-copy collective measurements for simultaneously estimating two non-commuting qubit rotations. This allows us to implement quantum-enhanced sensing, for which the metrological gain persists for high levels of decoherence, and to draw fundamental insights about the interpretation of the uncertainty principle. We implement our optimal measurements on superconducting, trapped-ion and photonic systems, providing an indication of how future quantum-enhanced sensing networks may look.

Quantum-enhanced single parameter estimation is an established capability, with non-classical probe states achieving precisions beyond what can be reached by the equivalent classical resources in photonic [1–3], trapped ion [4, 5], superconducting [6] and atomic [7, 8] systems. This has paved the way for quantum enhancements in practical sensing applications, from gravitational wave detection [9] to biological imaging [10]. For single-parameter estimation, entangled probe states are sufficient to reach the ultimate allowed precisions. However, for multi-parameter estimation, owing to the possible incompatibility of different observables, entangling resources are also required at the measurement stage. The ultimate attainable limits in quantum multi-parameter estimation are set by the Holevo Cramér-Rao bound (Holevo bound) [11, 12]. In most practical scenarios it is not feasible to reach the Holevo bound as this requires a collective measurement on infinitely many copies of the quantum state [13–16] (see Methods M1 for a rigorous definition of collective measurements). Nevertheless, it is important to develop techniques which will

enable the Holevo bound to be approached, given that multi-parameter estimation is fundamentally connected to the uncertainty principle [17] and has many physically motivated applications, including simultaneously estimating phase and phase diffusion [18, 19], quantum super-resolution [20, 21], estimating the components of a 3D field [22, 23] and tracking chemical processes [24]. Furthermore, as we demonstrate, collective measurements offer an avenue to quantum-enhanced sensing even in the presence of large amounts of decoherence, unlike the use of entangled probe states [25, 26].

To-date, collective measurements for quantum multi-parameter metrology have been demonstrated exclusively on optical systems [27–32]. Contemporary approaches to collective measurements on optical systems are limited in their scalability, i.e. it is difficult to generalise present approaches to measuring many copies of a quantum state simultaneously. The limited gate set available can also make it harder to implement an arbitrary optimal measurement. Indeed, the collective measurements demonstrated so far have all been restricted to measuring two copies of the quantum state and, while quantum enhancement has been observed, have all failed to reach the ultimate theoretical limits on separable measurements [33, 34]. Thus, there is a pressing need for a more

* lorcanconlon@gmail.com

† ping.lam@anu.edu.au

‡ cqtsma@gmail.com

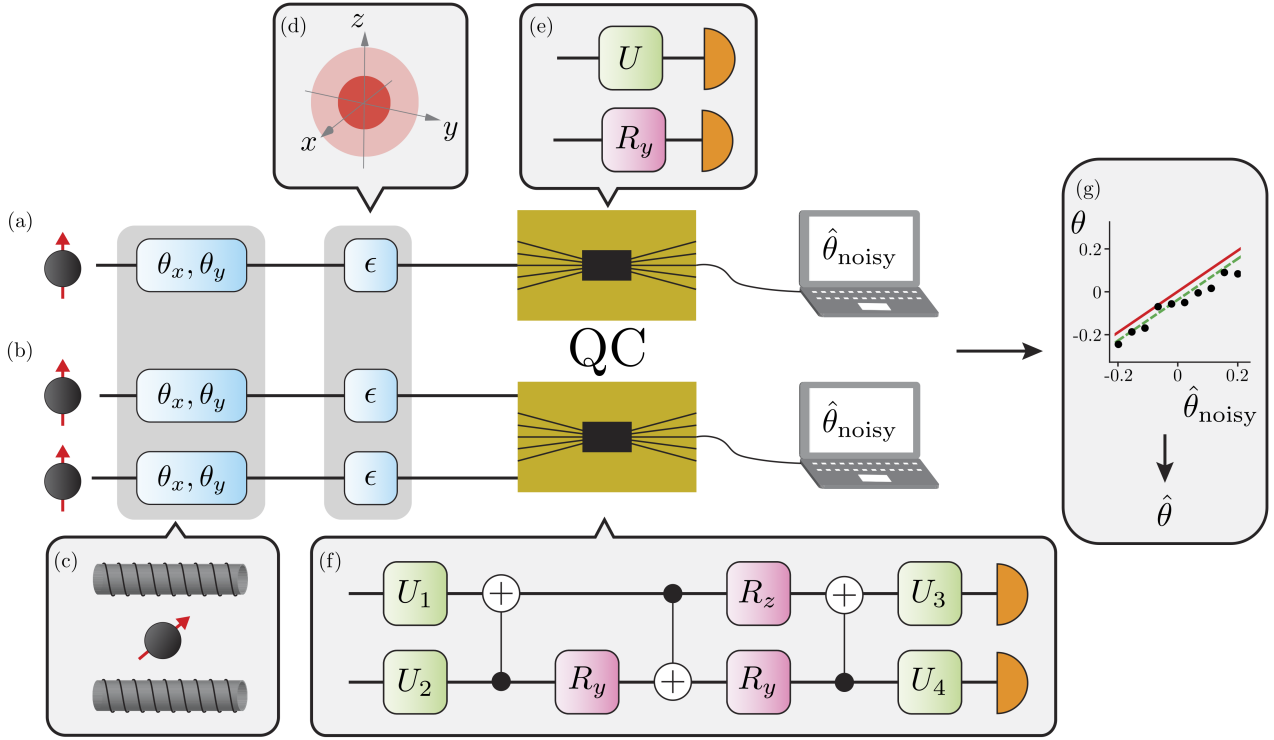


Figure 1: Experimental implementation of optimal collective measurements using quantum computers. Probe states are sent to the quantum computers (QC) individually for the single-copy measurement (a) and in pairs for the two-copy measurement (b). The qubit probes experience rotations, θ_x and θ_y , about the x and y axes of the Bloch sphere (c) before undergoing decoherence which has the effect of shrinking the Bloch vector (d). This rotation can be thought of as being caused by an external magnetic field which we wish to sense. The QCs then implement quantum circuits corresponding to the optimal single-copy (e) and two-copy (f) measurements. In (e) there are two optimal single-copy circuits, one for estimating θ_x and one for θ_y . Finally, error mitigation is used to improve the accuracy of the estimated angle (g). We create a model (green line) for how the noisy estimate of θ , $\hat{\theta}_{\text{noisy}}$ (black dots), is related to the true value (red line). The model is then used to correct $\hat{\theta}_{\text{noisy}}$ to produce the final estimate $\hat{\theta}$. Sample data from the F-IBM QS1 device downsampled by a factor of 3 is shown in (g). Error bars are smaller than the markers.

versatile and scalable approach to implementing collective measurements.

In this work we design and implement theoretically optimal collective measurement circuits on superconducting and trapped-ion platforms. The ease with which these devices can be reprogrammed, the universal gate set available, and the number of modes across which entanglement can be generated, ensure that they avoid many of the issues that current optical systems suffer from. Using recently developed error mitigation techniques [35] we estimate qubit rotations about the axes of the Bloch sphere with a greater precision than what is allowed by separable measurements on individual qubits. This approach allows us to investigate several interesting physical phenomena: i) We demonstrate both optimal single-copy and two-copy collective measurements reaching the theoretical limits [33, 34]. We also implement a three-copy collective measurement as a first step towards surpassing two-copy measurements. However, due to the circuit complexity, this measurement performs worse than single-copy measurements. ii) We investigate

the connection between collective measurements and the uncertainty principle. Using two-copy collective measurements, we experimentally violate a metrological bound based on known, but restrictive uncertainty relations [36]. iii) Finally, we compare the metrological performance of quantum processors from different platforms, providing an indication of how future quantum metrology networks may look.

Theoretical Results

In this work we implement theoretically optimal quantum circuits saturating the Nagaoka bound [33, 34], which sets an upper limit on the precision attainable with separable measurements. We consider the probe $|\psi\rangle = |0\rangle$, which experiences small rotations, θ_x and θ_y , about the x and y axes of the Bloch sphere respectively before getting decohered (Fig. 1 (c) and (d)). For small rotations, the state becomes $\rho_1 \approx (1 - \epsilon) |0\rangle \langle 0| + \epsilon/2 \mathbb{1}$, where ϵ is the decoherence strength. Such a noise model is relevant for quantum computing [37] and communica-

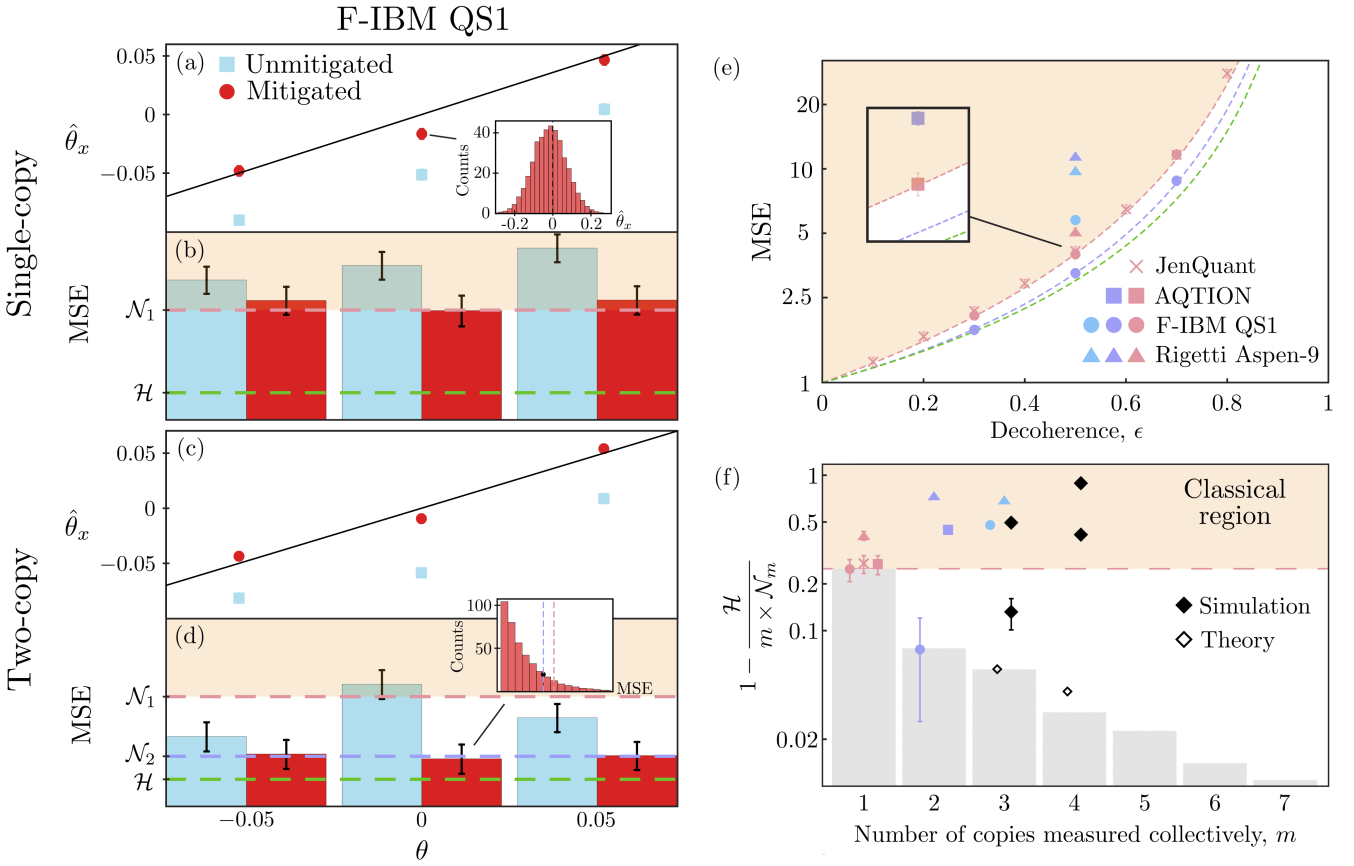


Figure 2: Surpassing single-copy limits through collective measurements. In all figures \dots , \dots and \dots correspond to the single-copy Nagaoka, two-copy Nagaoka and Holevo bounds respectively. The orange-shaded region corresponds to the mean squared error (MSE) attainable with separable measurements. MSEs below \dots are forbidden by quantum mechanics. Error bars are obtained using the bootstrapping technique [52] and correspond to one standard deviation. All experimental points have error bars but some are smaller than the marker size. Each data point corresponds to the average of 400 individual experimental runs, each using 512 shots, as shown in the inset of (a) (see Methods M4). (a) and (c) show single-copy and two-copy estimates of θ_x respectively, both with and without error mitigation. Results for estimating θ_y are similar (Extended Data Fig. 1). (b) and (d) show the corresponding MSE. The distribution of MSE values follows the expected chi-squared distribution, shown in the inset of (d). The black circle in the inset corresponds to the mean MSE value. The results shown in (a)-(d) are for decoherence parameter $\epsilon = 0.5$ and are obtained on the F-IBM QS1 device. (e) Optimal single-, two- and three-copy measurements at different decoherence strengths, ϵ . The pink, purple and blue markers correspond to experimental single-, two- and three-copy measurements respectively. For the superconducting devices all markers correspond to the precision after using error mitigation. The results of the AQTION trapped-ion processor for $\epsilon = 0.5$ are shown in the inset for clarity. (f) Bars are one minus the ratio of the Holevo bound to the m -copy Nagaoka bound, for m up to and including 7, calculated theoretically at $\epsilon = 0.5$. Experimental points are one minus the ratio of the Holevo bound to the MSE obtained experimentally. \diamond corresponds to the precision which our three- and four-copy projective measurements can obtain in theory. The upper and lower \blacklozenge are simulations based on a depolarising noise model with gate error rates of 5×10^{-3} and 1×10^{-3} respectively. Legend is the same as in (e).

tion [38] among other applications. The Nagaoka bound is given by

$$v_x + v_y \geq \mathcal{N}_1 = \frac{4}{(1-\epsilon)^2}, \quad (1)$$

where $v_{x(y)}$ is the variance in the estimate of $\theta_{x(y)}$. This applies when the probe states are measured one by one (Fig. 1 (a)). We shall refer to measurements of this type as *single-copy measurements*. The two-copy Nagaoka

bound is

$$v_x + v_y \geq \mathcal{N}_2 = \frac{4 - 2\epsilon + \epsilon^2}{2(1-\epsilon)^2}, \quad (2)$$

which applies when we can perform a collective measurement on two copies of the probe, $\rho_2 = \rho_1 \otimes \rho_1$, which are entangled during the measurement (Fig. 1 (b)). These measurements are referred to as *two-copy measurements*. Finally, allowing for collective measurements on infinitely

many copies of the probe state, the Holevo bound is

$$v_x + v_y \geq \mathcal{H} = \lim_{m \rightarrow \infty} m \times \mathcal{N}_m = \frac{4 - 2\epsilon}{(1 - \epsilon)^2}. \quad (3)$$

The hierarchy between the bounds is, $\mathcal{H} \leq 2\mathcal{N}_2 \leq \mathcal{N}_1$, with equality only for $\epsilon = 0$ or 1 . Detail on the computation of the different bounds is given in Supplementary Note 1.

The Nagaoka bounds, Eqs. (1) and (2), can be saturated by positive operator valued measures (POVMs) in 2- and 4-dimensional Hilbert spaces respectively (detailed in Supplementary Note 2). For single-copy measurements, it is possible to measure θ_x and θ_y separately, with two different POVMs, each using half of the total probe states without any loss in precision (Fig. 1 (e)). For the two-copy measurement this is not possible; both parameters have to be estimated simultaneously to take advantage of the collective measurement. In order to implement the optimal POVMs, we find a unitary matrix which diagonalises each POVM in the computational basis. Using standard techniques from quantum computing, we then convert these unitary matrices to quantum circuits [39], which can be executed experimentally (Fig. 1 (e) and (f)). We present three- and four-copy POVMs, and the corresponding quantum circuits, which theoretically surpass the two- and three-copy Nagaoka bounds respectively, in Supplementary Notes 3 and 4.

We also investigate the asymptotic attainability of the Holevo bound, examining how closely measurements on a finite number of copies of the probe state can approach it. In Fig. 2 (f), we compute the Nagaoka bound for performing collective measurements on up to 7 copies of the probe state simultaneously, corresponding to a 128-dimensional Hilbert space [40].

Experimental Results

In what follows we will describe the results of experiments conducted on multiple quantum platforms. The superconducting processors used were the Fraunhofer IBM Q System One (F-IBM QS1) processor, 11 cloud-accessible IBM Q processors and the Rigetti Aspen-9 processor. The trapped-ion (AQTION) processor is described in Ref. [41] and the Jena quantum photonic processor (JenQuant) is described in Methods M2. We implement the circuits corresponding to the optimal POVMs, shown in Fig. 1 (e) and (f), on the superconducting and trapped-ion processors. Additionally, we implement the single-copy measurements on JenQuant. The specific circuit parameters are provided in Supplementary Note 4. The outcomes of each run of a circuit are input to an estimator function to return the estimated values $\hat{\theta}_x$ and $\hat{\theta}_y$. This allows the mean squared error (MSE) to be determined.

Error Mitigation for Quantum Metrology

Our first experiment investigates one possible application of error mitigation to quantum metrology. The details of the error mitigation used are found in Methods M4, but it is essentially a calibration process based on known angles as shown in Fig. 1 (g). For this experiment, conducted on the F-IBM QS1 processor, the decoherence parameter is fixed at $\epsilon = 0.5$ and we estimate a range of θ values. This verifies the unbiasedness of the estimator after error mitigation. Fig. 2 (a) and (c) show the average estimate of θ_x , both before and after error mitigation, with single- and two-copy measurements respectively. The improvement offered by error mitigation, evident in these figures, is quantified by the MSE in Fig. 2 (b) and (d). Error mitigation cannot reduce the MSE below what is theoretically allowed by the Nagaoka bound, but it does enable both the single-copy and two-copy measurements to reach the corresponding Nagaoka bounds. Crucially, Fig. 2 (d) shows the advantage of the two-copy measurement, achieving a precision beyond what is classically possible over the range of θ considered. This is the first experimental demonstration of a measurement saturating the two-copy Nagaoka bound. Averaged over the entire range of θ , the two-copy measurements show a MSE $19 \pm 4\%$ below the theoretical single-copy measurement limit, which is only $6 \pm 4\%$ larger than the Holevo bound. In contrast, when restricted to single-copy measurements, the MSE is guaranteed to be at least 33% larger than the Holevo bound. The ability to measure a range of angles is important for practical applications of quantum-enhanced metrology.

Optimal Single-, Two- and Three-Copy Measurements

We next fix the rotations to $\theta_x = \theta_y = 0$ and demonstrate a quantum enhancement over a range of ϵ values. Fig. 2 (e) shows the (scaled) MSE attained on different platforms. Using the F-IBM QS1 device we are able to demonstrate a clear quantum enhancement across a range of ϵ values. The two-copy measurement on the F-IBM QS1 device shows a maximum advantage over the theoretical single-copy limit of $21 \pm 4\%$. In contrast, the Rigetti Aspen-9 superconducting device does not approach the theoretical limits for any of the measurements, likely due to the higher gate and readout error rates. Notably, both JenQuant and the AQTION processor are able to reach the theoretical single-copy measurement limits without any error mitigation. The AQTION processor does not however, reach the theoretical two-copy limits. The demonstration of quantum-enhanced sensing with highly mixed states showcases that collective measurements may provide metrological gain in real-world sensing applications where decoherence is unavoidable.

In Fig. 2 (e) and (f), we show the MSE of our three-copy measurement when implemented on the Rigetti Aspen-9 and F-IBM QS1 processors. In Supplementary

Note 6 we present further three-copy results for these and several other devices, all of which failed to reach the theoretical limit and display properties of a bad estimator. These experimental results are in qualitative agreement with simulations of three- and four-copy measurements based on the noise level expected for near-future quantum processors, also shown in Fig. 2 (f). From Fig. 2 (f), it is evident that for the problem we have considered, the benefit of three-copy measurements over two-copy measurements is marginal. This raises the question of whether measurements on many copies of a quantum state simultaneously are practically useful. In Supplementary Note 7 we present a similar problem, based on an amplitude damping noise model, where there is a sizeable gap between the two-copy Nagaoka and Holevo bounds, suggesting that collective measurements on many copies may be useful. With continually decreasing error rates, superconducting and trapped-ion devices may bridge this gap and approach the Holevo bound ever more closely. However, as the data from Fig. 2 (f) shows, there is a pertinent trade-off between what is gained by measuring more copies of the quantum state and what is lost by the increased experimental complexity.

Collective Measurements and the Uncertainty Principle

The uncertainty principle is one of the most fundamental features of quantum mechanics [17]. Recently, it has been observed that the original formulations of the uncertainty principle fail to hold in certain scenarios [42, 43], leading to the introduction of ‘universally valid’ uncertainty relations (UVUR) for operators [44–46]. In spite of the name, UVUR assume that measurements are carried out on single copies of the quantum state. This appears to be a natural assumption when considering how the measurement of one quantity disturbs any subsequent measurement of a second quantity. However, the same is not true when considering the precision with which two quantities can be jointly measured. Given this restriction, one might expect that UVUR can be violated through collective measurements.

Recently Lu and Wang extended the UVUR to quantum multi-parameter estimation [36], deriving a metrological bound on how well two parameters can be simultaneously estimated. We shall denote this as the LW uncertainty relation. For our problem this bound can be calculated as (see Supplementary Note 8)

$$\frac{1}{v_x} + \frac{1}{v_y} \leq (1 - \epsilon)^2, \quad (4)$$

which is saturated when $v_x = v_y = 2/(1 - \epsilon)^2$. The variances allowed by Eq. (4) coincide with our single-copy measurement variances. Indeed, our single-copy measurement variances, shown in pink in Fig. 3, verify the validity of UVUR in this scenario. However, our two-copy measurements implemented on the F-IBM QS1 processor were able to experimentally violate the LW uncertainty

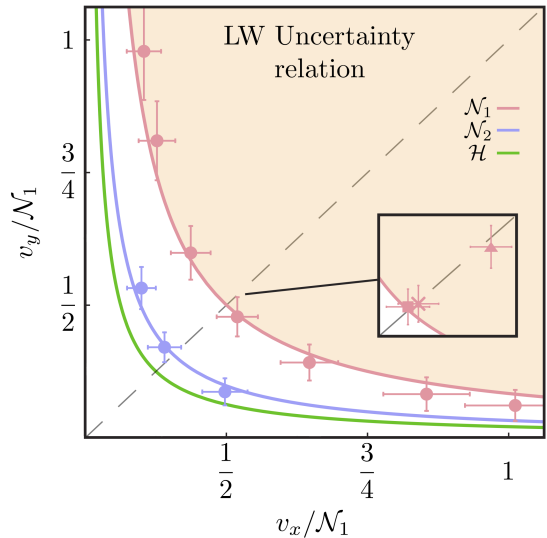


Figure 3: Collective measurements violating the LW uncertainty relation. The shaded region shows the measurement variances allowed by the LW uncertainty relation [36]. All experimental points correspond to a decoherence parameter of $\epsilon = 0.5$. The dashed grey line shows where the variance in estimating both parameters are equal. The purple and green lines are obtained by calculating the two-copy Nagaoka bound and Holevo bound with different weights attached to each parameter. Solid lines are used for bounds on the allowed values (v_x, v_y) (as opposed to the sum of variances as in Fig. 2). The data in the main figure corresponds to the F-IBM QS1 device. Data from the other processors is shown in the inset. The legend is the same as Fig. 2 (e). Each data point corresponds to the average of 400 individual experimental runs, each using 512 shots and error bars correspond to one standard deviation obtained by bootstrapping.

relation by more than 3 standard deviations as shown in purple in Fig. 3. The POVMs which give rise to the unbalanced variances are presented in Supplementary Note 9. To the best of our knowledge, this is the first time it has been observed that UVUR can be surpassed, either theoretically or experimentally. These results have significance for the manner in which the uncertainty principle is interpreted and suggest that tighter uncertainty relations are required when allowing for any measurement type. In Supplementary Note 10 we relate the violation of the LW uncertainty relation to the more common error-disturbance operator uncertainty relations.

Cross-platform Comparison

Our final experiment compares the performance of different platforms for estimating qubit rotations. This provides an indication of what resources may be used in a future quantum metrology network. For superconducting devices, we first perform simultaneous qubit rotation estimation using all non-neighbouring (pairs of) qubits,

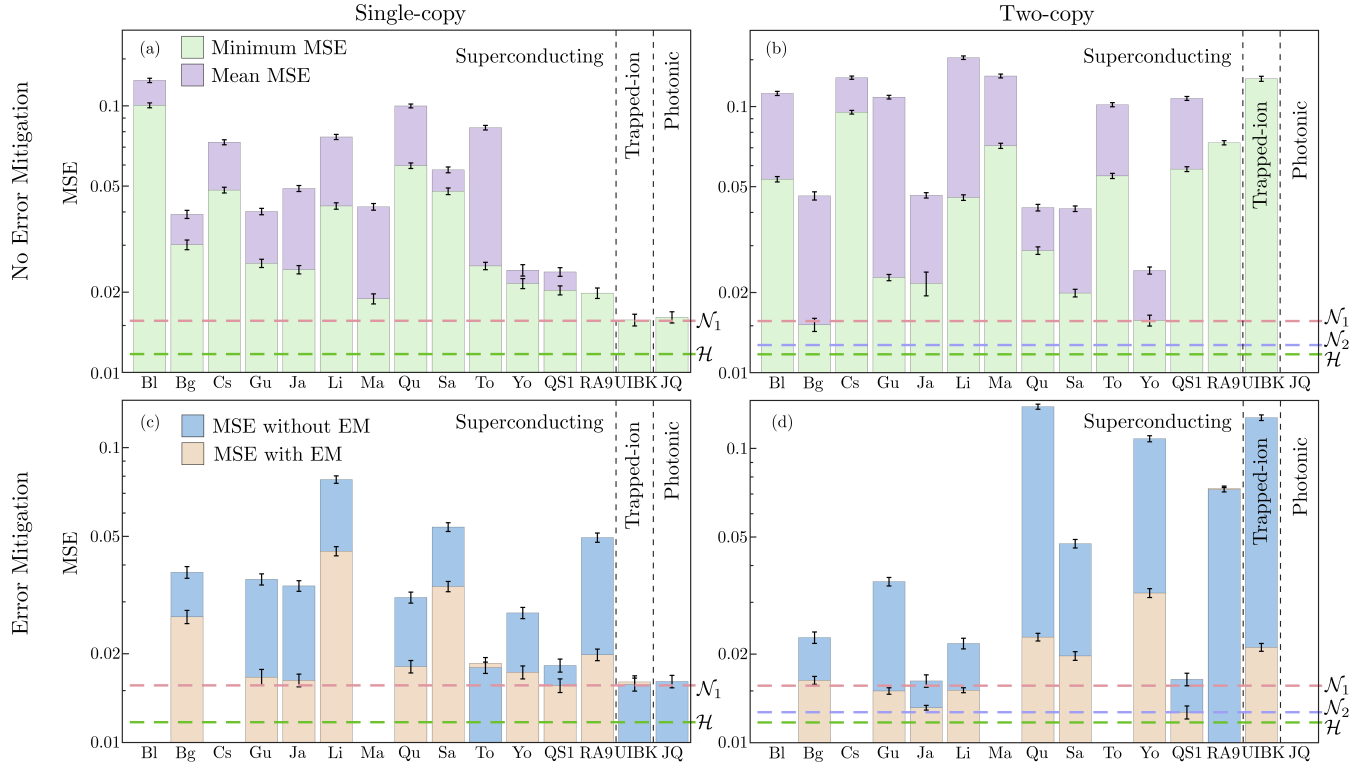


Figure 4: Comparing optimal measurement circuits on different quantum processors. (a) and (b) show the mean MSE and minimum MSE across all qubits with different quantum processors for the single-copy and two-copy measurements respectively. No error mitigation is used in these figures. Each MSE is averaged over 600 experimental runs, corresponding to 5 different angles, each using 512 shots. (c) and (d) show the MSE with and without error mitigation (EM) for the single-copy and two-copy measurements respectively. In all but four cases error mitigation is beneficial. The data in (c) and (d) corresponds to the average of 400 individual experimental runs, each using 512 shots. For all figures, error bars correspond to one standard deviation obtained by bootstrapping. The different IBM quantum computers tested are Belem (Bl), Bogota (Bg), Casablanca (Cs), Guadalupe (Gu), Jakarta (Ja), Lima (Li), Manhattan (Ma), Quito (Qu), Santiago (Sa), Toronto (To), Yorktown (Yo) and the F-IBM QS1 device (QS1). Also shown is the Rigetti Aspen-9 superconducting device (RA9), Jen-Quant (JQ) and the AQTION trapped-ion device (UBIK). For the Rigetti Aspen-9 device, only one qubit / pair of qubits was tested, hence the mean MSE and minimum MSE are equal. For the AQTION device the mean MSE and minimum MSE are equal as only one ion / pair of ions was loaded into the trap. Empty spaces correspond to processors where a particular experiment could not be carried out.

to minimise cross-talk between qubits. The mean MSE and minimum MSE across all qubits is shown in Fig. 4 (a) and (b) for each device tested. Each MSE is averaged over estimating 5 angles in the range $\theta = -0.01$ to 0.01 , repeated 120 times for each angle. For the trapped-ion and photonic devices only one photon, ion or pair of ions was used, hence only the mean MSE is shown. We then repeat the experiment using only the best performing qubit(s), now applying error mitigation as shown in Fig. 4 (c) and (d). The benefits of error mitigation are most pronounced for the F-IBM QS1 processor as we had unrestricted access to this device. Having restricted access to a device means each experiment takes longer, hence the model for the device provided by error mitigation is likely to be less accurate by the end of the experiment.

Discussion

Superconducting and trapped-ion devices are natural platforms for attaining the maximal advantage of quantum metrology and quantum information tasks through collective measurements. By implementing collective measurements on pairs of quantum states, we have been able to perform quantum multi-parameter estimation with a precision that cannot be reached classically using the same resources. There are many scenarios where this work may prove beneficial, particularly when there is an intrinsic restriction on resources. One can envision an optical system connected to a quantum processor through optical-to-microwave converters [47]. With only a limited number of qubits, such a device could greatly enhance biomedical imaging or quantum communications, meaning these advantages may be leveraged with near-future technology. Furthermore, collect-

ive measurements can be beneficial for quantum tomography [48], entanglement distillation for quantum communication [49] and quantum illumination [50].

This work opens up a number of avenues for future investigation: a natural extension to using error mitigation for quantum metrology is error correction [51]. With the aid of the techniques presented here, it may be possible to demonstrate multi-parameter metrology which fully utilises quantum resources; benefiting from both entangled probe states and collective measurements. By simplifying our three-copy measurement circuit, the theoretical limits may be approachable with the present generation of quantum processors. It would also be pertinent to study further how gate error rates and circuit complexity need to scale to successfully implement many-copy collective measurements. Investigating further the connection between collective measurements and the uncertainty principle may reveal important aspects of fundamental physics and could lead to the development of tighter uncertainty relations which hold true for any measurement type. Finally, the ideal extension of our work is to demonstrate optimal collective measurements in a practical setting. We anticipate that our work brings this closer.

ACKNOWLEDGEMENTS

We acknowledge the use of IBM Quantum services and the Rigetti Aspen-9 processor for this work. The views expressed are those of the authors, and do not reflect the official policy or position of IBM, the IBM Quantum team or Rigetti.

The authors would like to acknowledge the support of Amazon Web Services by making available the Rigetti Aspen-9 device using the Amazon Braket service.

This research was funded by the Australian Research Council Centre of Excellence CE170100012, Laureate Fellowship FL150100019 and the Australian Government Research Training Program Scholarship.

This work has been supported by the Fraunhofer-Gesellschaft zur Förderung der angewandten Forschung e.V. We gratefully acknowledge the financial support

by the German Federal Ministry of Education and Research via ‘2D Nanomaterialien für die Nanoskopie der Zukunft’, FKZ: 13XP5053A and the European Union, the European Social Funds and the Federal State of Thuringia under Grant ID 2021FGI0043.

This work was funded by the Deutsche Forschungsgemeinschaft (DFG, German Research Foundation) - Projekt-Nr. 445275953. The authors acknowledge support by the German Space Agency DLR with funds provided by the Federal Ministry for Economic Affairs and Energy BMWi under grant number 50WM2165 (QUICK3).

DWB is supported by Australian Research Council Discovery Projects DP190102633 and DP210101367.

CDM, IP, and TM acknowledge funding from the EU H2020-FETFLAG-2018-03 under Grant Agreement no. 820495. We also acknowledge support by the Austrian Science Fund (FWF), through the SFB BeyondC (FWF Project No. F7109), and the IQI GmbH, as well as the Office of the Director of National Intelligence (ODNI), Intelligence Advanced Research Projects Activity (IARPA), via US ARO grant no. W911NF-16-1-0070 and W911NF-20-1-0007, and the US Air Force Office of Scientific Research (AFOSR) via IOE Grant No. FA9550-19-1-7044 LASCEM.

AUTHOR CONTRIBUTIONS

PKL conceived the project. LC and SMA derived the theoretical results and designed the optimal quantum circuits. LC, DWB and SMA optimised the quantum circuits. TV ran the JenQuant experiment. CDM and IP ran the AQTION experiment. LC and FE ran the F-IBM QS1 experiment. LC performed the data analysis. LC, SY and SMA derived the bounds in Fig. 3. LC wrote the manuscript with contributions from all authors.

COMPETING INTERESTS

The authors declare no competing interests.

[1] Kacprowicz, M., Demkowicz-Dobrzański, R., Wasilewski, W., Banaszek, K. & Walmsley, I. Experimental quantum-enhanced estimation of a lossy phase shift. *Nat. Photonics* **4**, 357–360 (2010).

[2] Slussarenko, S. *et al.* Unconditional violation of the shot-noise limit in photonic quantum metrology. *Nat. Photonics* **11**, 700–703 (2017).

[3] Guo, X. *et al.* Distributed quantum sensing in a continuous-variable entangled network. *Nat. Phys.* **16**, 281–284 (2020).

[4] McCormick, K. C. *et al.* Quantum-enhanced sensing of a single-ion mechanical oscillator. *Nature* **572**, 86–90 (2019).

[5] Leibfried, D. *et al.* Toward Heisenberg-limited spectroscopy with multiparticle entangled states. *Science* **304**, 1476–1478 (2004).

[6] Wang, W. *et al.* Heisenberg-limited single-mode quantum metrology in a superconducting circuit. *Nat. Commun.* **10**, 1–6 (2019).

[7] Muessel, W., Strobel, H., Linnemann, D., Hume, D. & Oberthaler, M. Scalable spin squeezing for quantum-enhanced magnetometry with Bose-Einstein condensates. *Phys. Rev. Lett.* **113**, 103004 (2014).

[8] Gross, C., Zibold, T., Nicklas, E., Esteve, J. & Oberthaler, M. K. Nonlinear atom interferometer surpasses classical precision limit. *Nature* **464**, 1165–1169 (2010).

[9] Aasi, J. *et al.* Enhanced sensitivity of the LIGO gravitational wave detector by using squeezed states of light. *Nat. Photonics* **7**, 613–619 (2013).

[10] Casacio, C. A. *et al.* Quantum-enhanced nonlinear microscopy. *Nature* **594**, 201–206 (2021).

[11] Holevo, A. S. Statistical decision theory for quantum systems. *J. Multivar. Anal.* **3**, 337–394 (1973).

[12] Holevo, A. S. *Probabilistic and statistical aspects of quantum theory*, vol. 1 (Springer Science & Business Media, 2011).

[13] Kahn, J. & Guță, M. Local asymptotic normality for finite dimensional quantum systems. *Commun. Math. Phys.* **289**, 597–652 (2009).

[14] Yamagata, K., Fujiwara, A. & Gill, R. D. Quantum local asymptotic normality based on a new quantum likelihood ratio. *Ann. Stat.* **41**, 2197–2217 (2013).

[15] Yang, Y., Chiribella, G. & Hayashi, M. Attaining the ultimate precision limit in quantum state estimation. *Commun. Math. Phys.* **368**, 223–293 (2019).

[16] Conlon, L. O., Suzuki, J., Lam, P. K. & Assad, S. M. The gap persistence theorem for quantum multiparameter estimation. *arXiv preprint arXiv:2208.07386* (2022).

[17] Heisenberg, W. Über den anschaulichen Inhalt der quantentheoretischen Kinematik und Mechanik. In *Original Scientific Papers Wissenschaftliche Originalarbeiten*, 478–504 (Springer, 1985).

[18] Vidrighin, M. D. *et al.* Joint estimation of phase and phase diffusion for quantum metrology. *Nat. Commun.* **5**, 1–7 (2014).

[19] Szczykulska, M., Baumgratz, T. & Datta, A. Reaching for the quantum limits in the simultaneous estimation of phase and phase diffusion. *Quantum Sci. Technol.* **2**, 044004 (2017).

[20] Řeháček, J. *et al.* Multiparameter quantum metrology of incoherent point sources: towards realistic superresolution. *Phys. Rev. A* **96**, 062107 (2017).

[21] Chrostowski, A., Demkowicz-Dobrzański, R., Jarzyna, M. & Banaszek, K. On super-resolution imaging as a multiparameter estimation problem. *Int. J. Quantum Inf.* **15**, 1740005 (2017).

[22] Baumgratz, T. & Datta, A. Quantum enhanced estimation of a multidimensional field. *Phys. Rev. Lett.* **116**, 030801 (2016).

[23] Hou, Z. *et al.* Minimal tradeoff and ultimate precision limit of multiparameter quantum magnetometry under the parallel scheme. *Phys. Rev. Lett.* **125**, 020501 (2020).

[24] Cimini, V. *et al.* Quantum sensing for dynamical tracking of chemical processes. *Phys. Rev. A* **99**, 053817 (2019).

[25] Dorner, U. *et al.* Optimal quantum phase estimation. *Phys. Rev. Lett.* **102**, 040403 (2009).

[26] Demkowicz-Dobrzański, R., Kołodyński, J. & Guță, M. The elusive Heisenberg limit in quantum-enhanced metrology. *Nat. Commun.* **3**, 1–8 (2012).

[27] Roccia, E. *et al.* Entangling measurements for multiparameter estimation with two qubits. *Quantum Sci. Technol.* **3**, 01LT01 (2017).

[28] Parniak, M. *et al.* Beating the Rayleigh limit using two-photon interference. *Phys. Rev. Lett.* **121**, 250503 (2018).

[29] Hou, Z. *et al.* Deterministic realization of collective measurements via photonic quantum walks. *Nat. Commun.* **9**, 1–7 (2018).

[30] Wu, K.-D. *et al.* Experimentally reducing the quantum measurement back action in work distributions by a collective measurement. *Sci. Adv.* **5**, eaav4944 (2019).

[31] Yuan, Y. *et al.* Direct estimation of quantum coherence by collective measurements. *npj Quantum Inf.* **6**, 1–5 (2020).

[32] Wu, K.-D. *et al.* Minimizing backaction through entangled measurements. *Phys. Rev. Lett.* **125**, 210401 (2020).

[33] Nagaoka, H. A new approach to Cramér-Rao bounds for quantum state estimation. In *Asymptotic Theory Of Quantum Statistical Inference: Selected Papers*, 100–112 (2005). Originally published as IEICE Technical Report, 89, 228, IT 89-42, 9-14, (1989).

[34] Nagaoka, H. A generalization of the simultaneous diagonalization of Hermitian matrices and its relation to quantum estimation theory. In *Asymptotic Theory Of Quantum Statistical Inference: Selected Papers*, 133–149 (World Scientific, 2005). Originally published as Trans. Jap. Soc. Indust. Appl. Math., 1, 43–56, (1991) in Japanese. Translated to English by Y. Tsuda.

[35] Czarnik, P., Arrasmith, A., Coles, P. J. & Cincio, L. Error mitigation with Clifford quantum-circuit data. *Quantum* **5**, 592 (2021).

[36] Lu, X.-M. & Wang, X. Incorporating Heisenberg's uncertainty principle into quantum multiparameter estimation. *Phys. Rev. Lett.* **126**, 120503 (2021).

[37] Vovrosh, J. *et al.* Simple mitigation of global depolarizing errors in quantum simulations. *Phys. Rev. E* **104**, 035309 (2021).

[38] Bennett, C. H., Shor, P. W., Smolin, J. A. & Thapliyal, A. V. Entanglement-assisted classical capacity of noisy quantum channels. *Phys. Rev. Lett.* **83**, 3081 (1999).

[39] Vatan, F. & Williams, C. Optimal quantum circuits for general two-qubit gates. *Phys. Rev. A* **69**, 032315 (2004).

[40] Conlon, L. O., Suzuki, J., Lam, P. K. & Assad, S. M. Efficient computation of the Nagaoka–Hayashi bound for multiparameter estimation with separable measurements. *npj Quantum Inf.* **7**, 1–8 (2021).

[41] Pogorelov, I. *et al.* Compact ion-trap quantum computing demonstrator. *PRX Quantum* **2**, 020343 (2021).

[42] Erhart, J. *et al.* Experimental demonstration of a universally valid error-disturbance uncertainty relation in spin measurements. *Nat. Phys.* **8**, 185–189 (2012).

[43] Rozema, L. A. *et al.* Violation of Heisenberg's measurement-disturbance relationship by weak measurements. *Phys. Rev. Lett.* **109**, 100404 (2012).

[44] Ozawa, M. Universally valid reformulation of the Heisenberg uncertainty principle on noise and disturbance in measurement. *Phys. Rev. A* **67**, 042105 (2003).

[45] Ozawa, M. Uncertainty relations for joint measurements of noncommuting observables. *Phys. Lett. A* **320**, 367–374 (2004).

[46] Branciard, C. Error-tradeoff and error-disturbance relations for incompatible quantum measurements. *Proc. Natl. Acad. Sci.* **110**, 6742–6747 (2013).

[47] Higginbotham, A. P. *et al.* Harnessing electro-optic correlations in an efficient mechanical converter. *Nat. Phys.* **14**, 1038–1042 (2018).

[48] Massar, S. & Popescu, S. Optimal extraction of information from finite quantum ensembles. *Phys. Rev. Lett.* **74**, 1259–1263 (1995).

- [49] Bennett, C. H. *et al.* Purification of noisy entanglement and faithful teleportation via noisy channels. *Phys. Rev. Lett.* **76**, 722 (1996).
- [50] Zhuang, Q., Zhang, Z. & Shapiro, J. H. Optimum mixed-state discrimination for noisy entanglement-enhanced sensing. *Phys. Rev. Lett.* **118**, 040801 (2017).
- [51] Dür, W., Skotiniotis, M., Froewis, F. & Kraus, B. Improved quantum metrology using quantum error correction. *Phys. Rev. Lett.* **112**, 080801 (2014).
- [52] Rice, J. A. *Mathematical statistics and data analysis* (Cengage Learning, 2006).

METHODS

M1. Collective measurements

Here we clarify our use of terminology regarding ‘entangling’ and ‘collective’ measurements. We stick to the definitions used in Refs. [27–32], where a collective measurement is a measurement that acts on multiple copies of the quantum state simultaneously. An N -copy collective measurement thus simultaneously measures N copies of the same state, whereas a ‘single-copy’ measurement, or ‘separable’ measurement, measures the quantum states individually. The quantum states themselves may consist of an arbitrary number of possibly entangled modes. When we refer to ‘entangling’ measurements we mean measurements capable of creating entanglement between *multiple copies* of the quantum state, or alternatively, in an entangled multi-copy basis.

There are many similar concepts, which may be confused with our definition of a collective measurement. For example: In Ref. [53] a quantum state with 26 entangled modes (ions) was used. In our terminology, measuring the 26 ions simultaneously is a separable measurement, because only a single copy of the quantum state was used and consequently no entanglement between copies was possible. However, in principle the (0,2) and (1,2) schemes in Ref. [53] could be used for implementing collective measurements in the sense of our definition. Similarly, Ref. [54] refers to collective measurements as measurements of ensemble quantities of atoms, wholly unrelated to our terminology. In Ref. [55] multi-copy discrimination of two quantum states is demonstrated. However, this multi-copy discrimination uses separable measurements, the multi-copy part referring to the fact that multiple (separable) measurement outcomes are used in making a final decision. Finally, Refs. [56, 57] examine multi-copy metrology. Again in this work, the term multi-copy carries a different meaning compared to our work, as only single parameter estimation was considered.

M2. Photonic experiment

The Jena quantum photonic processor (JenQuant) is based on a single photon emitting colour centre in the two-dimensional material hexagonal boron nitride

(hBN). The crystal defect introduces an effective two-level system into the bandgap that is excited optically. The emitter is fabricated by treating a multilayer hBN crystal with an oxygen plasma and subsequent rapid thermal annealing [58]. A suitable quantum emitter was then coupled to a hemispherical microcavity [59]. The resonator enhances the emission via the Purcell effect and suppresses noise to reduce the multi-photon probability below 0.6% at room temperature [60]. The spectrum is tunable by adjusting the resonator length within the free space emission linewidth of 5.76 nm (FWHM) around 565 nm and has a linewidth of 0.2 nm [59].

We encode the logical qubits in the polarisation of the photons and choose $|H/V\rangle$ as the computational basis states $|0/1\rangle$. The input states $|0\rangle$, $|1\rangle$, and $|\psi_\theta\rangle$ are set by motorized polarisation optics (a half-wave plate (HWP), polariser, and a quarter-wave plate (QWP)). The polariser ensures a high polarisation extinction ratio of $> 10^5:1$. The single-copy POVMs are implemented by the combination of motorized QWP, HWP, QWP, which can perform any arbitrary unitary rotation. In Supplementary Note 4 we show the decomposition of the optimal single-copy POVMs into wave plate rotations. Finally, a polarising beam splitter projects onto the computational basis and the photons are detected by two single photon detectors in both arms. JenQuant is thereby a fully universal single qubit quantum computer. Performing multi-qubit operations requires an entangling gate such as CNOT which would require indistinguishable single photons. This in turn can be achieved by a narrower resonator linewidth < 124 MHz to reach a Hong-Ou-Mandel contrast $> 90\%$ [59]. Note that JenQuant does not require any error mitigation, partly due to the long-term stability of the system.

M3. Superconducting experiments

The F-IBM QS1 device used is based in Ehningen. It uses an IBM Quantum Falcon processor and has 27 qubits. As with all IBM Quantum devices, the qubits are transmons. The frequency of the transmons are around 5 GHz [61].

M4. Error mitigation

Before running each experiment for estimating the unknown angles θ_x and θ_y , we implement Clifford data regression error mitigation [35]. This involves constructing a model for how a noisy expectation value predicted by a quantum processor is related to the true expectation value. In general complex models can be used, however, for quantum metrology, it is essential that the chosen model does not bias the estimator. We are therefore required to use a simple model of the form $\hat{\theta}_{x(y)} = \hat{\theta}_{\text{noisy}, x(y)} + c_{x(y)}$, where $\hat{\theta}_{\text{noisy}, x(y)}$ is the unmitigated $\theta_{x(y)}$ value predicted by the quantum processor

and $c_{x(y)}$ is a constant. Detail on other possible models which were considered, but found to bias the estimator, is provided in Supplementary Note 5. We use 30 known θ values in the range $\theta \in [-0.2, 0.2]$ rad to determine a value for the model $c_{x(y)}$. An example of the model fitting is shown in Fig. 1 (g) for the F-IBM QS1 quantum processor. This model is then used to estimate some unknown angle $\theta = \theta_x = \theta_y$. Unless otherwise specified in the main text, the model is recalibrated after every 40 predictions of the unknown angle and the process is repeated to estimate each unknown angle 400 times. Our figure of merit is taken to be the average MSE over all 400 runs.

$$\text{MSE} = \frac{1}{400} \sum_{i=1}^{400} ((\theta_x - \hat{\theta}_{x,i})^2 + (\theta_y - \hat{\theta}_{y,i})^2), \quad (5)$$

where $\hat{\theta}_{x(y),i}$ is the i th estimate of $\theta_{x(y)}$. To obtain each of the 400 estimates we average the results of 512 repetitions of the experiment for each of the single-copy circuits and for the two-copy circuit. For the three-copy circuit we average the results of 341 repetitions of the experiment to ensure equal resources are used in each experiment.

For the two-copy measurements in Fig. 3 with $v_x \neq v_y$, a slightly different error mitigation process was used. At the time this particular data was being taken it was

not possible to recalibrate in between estimating the unknown angle. Hence, the calibration step was only performed once, immediately before estimating the unknown angle. To increase the utility of the error mitigation in this case, we used 30 known angles in the range $\theta \in [-0.05, 0.05]$ rad.

DATA AVAILABILITY

All data and codes are available at the following Github repository: <https://github.com/LorcanConlon/Approaching-optimal-entangling-collective-measurements>.

CODE AVAILABILITY

All data and codes are available at the following Github repository: <https://github.com/LorcanConlon/Approaching-optimal-entangling-collective-measurements>.

EXTENDED DATA

[53] Marciak, Ch. D. *et al.* Optimal metrology with programmable quantum sensors. *Nature* **603**, 604–609 (2022).

[54] Bohnet, J. G. *et al.* Reduced spin measurement back-action for a phase sensitivity ten times beyond the standard quantum limit. *Nat. Photonics* **8**, 731–736 (2014).

[55] Jagannathan, A. *et al.* Demonstration of quantum-limited discrimination of multicopy pure versus mixed states. *Phys. Rev. A* **105**, 032446 (2022).

[56] Tóth, G., Vértesi, T., Horodecki, P. & Horodecki, R. Activating hidden metrological usefulness. *Phys. Rev. Lett.* **125**, 020402 (2020).

[57] Trényi, R. *et al.* Multicopy metrology with many-particle quantum states. *arXiv preprint arXiv:2203.05538* (2022).

[58] Vogl, T., Campbell, G., Buchler, B. C., Lu, Y. & Lam, P. K. Fabrication and deterministic transfer of high-quality quantum emitters in hexagonal boron nitride. *ACS Photonics* **5**, 2305–2312 (2018).

[59] Vogl, T., Lecamwasam, R., Buchler, B. C., Lu, Y. & Lam, P. K. Compact cavity-enhanced single-photon generation with hexagonal boron nitride. *ACS Photonics* **6**, 1955–1962 (2019).

[60] Vogl, T., Knopf, H., Weissflog, M., Lam, P. K. & Eilenberger, F. Sensitive single-photon test of extended quantum theory with two-dimensional hexagonal boron nitride. *Phys. Rev. Res.* **3**, 013296 (2021).

[61] Jurcevic, P. *et al.* Demonstration of quantum volume 64 on a superconducting quantum computing system. *Quantum Sci. Technol.* **6**, 025020 (2021).

[62] Temme, K., Bravyi, S. & Gambetta, J. M. Error mitigation for short-depth quantum circuits. *Phys. Rev. Lett.* **119**, 180509 (2017).

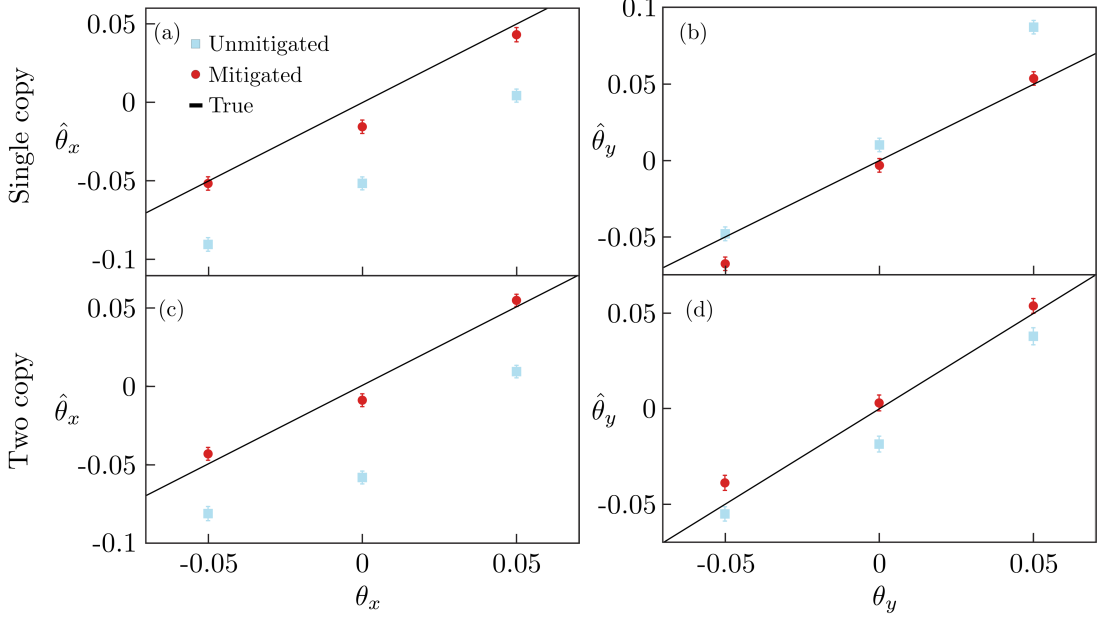


Figure 5: Effect of error mitigation on estimation performance. Figs (a) to (d) show the estimated values of θ , averaged over all 400 runs, before (blue squares) and after (red circles) applying error mitigation. Figs (a) and (b) ((c) and (d)) correspond to estimating θ_x and θ_y respectively with the optimal single(two)-copy measurement. Error bars are obtained using the bootstrapping technique [52] and correspond to one standard deviation. All results shown are for decoherence parameter $\epsilon = 0.5$ and are obtained on the F-IBM QS1 device.